Interaction of energetic oxygen ions with the beryllium tungsten alloy Be_2W

M. Köppen, J. Riesch, A. Vollmer*, and Ch. Linsmeier

Max-Planck-Institut für Plasmaphysik, EURATOM Association, Boltzmannstr. 2, 85748 Garching b. München, Germany

* *Helmholtz Zentrum Berlin für Materialien und Energie GmbH, Wilhelm-Conrad-Röntgen Campus BESSY II, Albert-Einstein-Str. 15, 12489 Berlin, Germany*

Abstract

In this study the interaction of energetic oxygen ions with the beryllium-tungsten alloy Be_2W is investigated by depth-resolved X-ray photo-electron spectroscopy (XPS). A 4 nm tungsten layer is deposited on polycrystalline beryllium. By alloying at 900 K for 60 min Be_2W is formed. In successive steps oxygen ions are implanted with 500 and 1000 V acceleration voltage with a fluence of $5 \cdot 10^{14}$ cm^{-2} in each step. Between the single implantation steps the sample is heated for 30 min at 600 K. Depth-resolved photoelectron spectroscopy is performed after each experimental step. The W $4f$ and Be $1s$ spectra reveal formation of beryllium tungstate $BeWO_4$ already at room temperature (r.t.) in significant amounts due to energy deposition of implanted oxygen ions. No indication for oxygen diffusion at r.t. is observed. In previous experiments in thermal equilibrium the ternary compound has proven to be stable to temperatures up to 1073 K. Contrary to these results, annealing at 600 K already leads to decomposition of $BeWO_4$ formed by energetic oxygen ions. After decomposition at 600 K oxygen stays in the sample bound as BeO.

1 Introduction

The three elements beryllium, carbon and tungsten are planned as armour material covering the inner wall of the vacuum vessel of the future fusion device ITER [1]. During operation wall material is eroded from the plasma-facing surfaces due to elevated temperatures or sputtering by energetic species. Eroded wall material is transported along the magnetic field lines and re-deposited at different locations, forming layers on the wall tiles. Since approx. 700 m^2 of the first wall are covered by beryllium, deposition of Be on tungsten tiles is one possible consequence. Due to the elevated temperatures at the first wall these thin layers are alloyed with W and form Be_2W. Contamination of the surfaces and the plasma by oxygen is inevitable after the vacuum vessel is exposed to air, e.g. for maintenance. Oxygen leaving the plasma is implanted into the wall material. Its kinetic energy can trigger chemical reactions with the wall materials. Additional thermally activated reactions will take place due to elevated wall temperatures at ITER. Knowledge of the processes at the first wall is crucial to predict the dynamic change of the ITER plasma-facing surface composition. Newly formed phases show different physical properties compared to the original surface, e.g. melting point, thermal conductivity and hydrogen retention. In particular, formed oxides can have great influence since their melting points vary over a huge range. While metallic tungsten has a melting point of 3683 K, its two stoichiometric oxides WO_3 and WO_2 already melt at 1746 K and 1773 K. Beryllium, on the contrary, shows an increase in its melting point after oxidation from 1551 K to 2780 K. Previous studies have dealt with various binary systems containing Be, C and W [2]. The next step is to increase the number of reaction paths by adding more elements to the reaction scenario and identification of the reactions in the more complex systems.

Former experiments have shown complex chemistry between Be, O and W in thermally induced reactions. The ternary compounds beryllium tungsten bronze Be_xWO_3 and beryllium tungstate $BeWO_4$ were observed in the system Be on WO_3. It was found that Be_xWO_3 reaches its maximum at 573 K and decomposes at 873 K, while the tungstate reaches its maximum at 973 K and a complete decomposition could not be observed for temperatures up to 1273 K [3].

In this study, the interaction of energetic oxygen ions with the beryllium-tungsten alloy Be_2W is investigated by depth-resolved X-ray photoelectron spectroscopy (XPS).

2 Experiment

In depth-resolved XPS the information depth is varied by using different photon energies to excite the photoelectrons from core levels. According to $E_{kin} = h\nu - E_b - \phi_a$, a higher photon energy $h\nu$ results in a higher kinetic energy of the photoelectron E_{kin} for a given binding energy E_b. The work function of the analyser ϕ_a is determined for each spectrum by a Au $4f_{7/2}$ reference measurement. Since the inelastic mean free path of electrons is energy dependent, it is possible to change the information depth by using different photon energies [4]. In order to measure identical information depths for all core levels of interest, the photon energy is tuned such, that the resulting kinetic energy of photoelectrons for the W 4*f*, Be 1*s* and O 1*s* levels is identical.

All experiments are carried out at the synchrotron facility HZB-BESSY II at the end-station SurICat, which is specialised in photoemission experiments with photon energies ranging from 20 to 1300 eV. Our sample preparation chamber LAICA is directly interconnected to the analysis chamber. LAICA is dedicated for sample synthesis for experiments with the ITER material mix, featuring three electron beam evaporators for Be, C and W, an ion gun for sample cleaning and implantation experiments with acceleration energies up to 5 keV, an electron bombardment heater for sample heating up to 1370 K, and an Auger electron spectroscopy (AES) system. Base pressures in the preparation chamber are well below $1 \cdot 10^{-9}$ hPa and in the analysis chamber $1 \cdot 10^{-10}$ hPa.

A 4 nm W layer is deposited by physical vapour deposition on a polycrystalline Be disc with 10 mm diameter. The Be surface is previously cleaned cyclically by Ar^+ sputtering at 3 keV and annealing at 600 K until no C and O signals can be detected by AES. The sample is alloyed at 900 K for 60 min to form a Be_2W layer. The O implantation energies for these experiments are chosen such that implantation range is within the accessible depth for XPS at the available photon energies. It is assumed that the O ion beam consists of two ionic O species O^+ and O_2^+. In these experiments the exact composition of the ion beam cannot be determined. Therefore, for the simulation and the fluence calculations the beam composition was assumed to be 82 % O_2^+ and 18 % O^+. These values are taken from a mass spectrum of O_2 ionised by electron impact [5]. Since the used ion source uses the same ionisation method, these ion fractions should be a valid approximation. Electrons with an energy of about 100 eV are used for ionisation of O_2. The O_2 pressure in the ioniser section of the ion source is approx.

$5 \cdot 10^{-6}$ hPa, resulting in an O_2-pressure of $2 \cdot 10^{-7}$ hPa in the preparation chamber during implantation. Implantation profiles are simulated using the program SDTrim.SP [6, 7]. According to simulations, acceleration voltages of up to 1000 V satisfy the range requirement for O fluences of $5 \cdot 10^{14}$ cm^{-2}. After O implantation with 1 kV acceleration voltage the XP spectra show, that the maximum information depth is aready utilised by implanted O. Therefore, a lower acceleration voltage of 500 V is used for the following two implantation steps. This renders the observation of possible diffusive processes towards the bulk possible. Calculated implantation profiles are shown in Fig. 1. The maximum implantation depths are 5 nm for 500 eV and 7.5 nm for 1000 eV implantation energies, respectively. In short, the sequence of experimental steps is:

1. Cleaning of Be-disc
2. Evaporation of W on Be
3. Alloying at 900 K for 60 min
4. O-Implantation with 1000 V
5. Annealing at 600 K for 30 min
6. First O-Implantation with 500 V
7. Annealing at 600 K for 30 min
8. Second O-Implantation with 500 V

Between single implantation steps the sample is annealed at 600 K for 30 min. This temperature is chosen, because we found in former experiments with Be on WO_3 beginning formation of $BeWO_4$ at this temperature. Photoelectron spectra are taken after each experimental step. High resolution spectra of core levels of every element present are taken at up to six different information depths. Kinetic energies of photoelectrons, respective photon energies for the investigated core levels and the IMFPs calculated after Seah and Dench [8] are compiled in Tab. 1. In addition, survey scans with photon energies of 655 and 990 eV are measured to identify the elements present at the sample.

Binding energy (BE) scales of the spectra are referenced to the Au $4f_{7/2}$ peak with a binding energy of 84.0 eV. The following equation gives all contribution to the XPS intensity:

$$I = \sigma \cdot L \cdot J \cdot D \cdot T \cdot \int_{z=0}^{\infty} \rho(z) \exp\left[-\frac{z}{\lambda \cos\alpha}\right] \tag{1}$$

After dividing the spectra yield by photon flux J, asymmetry parameter L and photo-ionisation cross-sections σ after Yeh [9], analyser transmission T, and detector efficiency D given by the manufacturer, only the integral over the depth-dependent atomic density $\rho(z)$ remains. The exponential function here gives the weighting of the density in dependence to its depth z, taking into account the inelastic electron mean free path λ and the angle α between the surface normal and the analyzer ($\alpha = 0°$ in our experiment). In other words, the closer an atom is located to the surface, the higher is its contribution to the measured intensity I.

The background in the XP-spectra is subtracted by applying a Tougaard-style background [10]. Peaks are fitted using a Doniach-Šunjić-type function [11]. During the fitting procedure of the W $4f$ spectra, the doublet separation between the W $4f_{5/2}$ and W $4f_{7/2}$ peaks is held constant at 2.18 eV.

3 Results

In this section the observations in the single spectral regions are described. Please note, that energies given for the W $4f$ spectra always refer to the W $4f_{7/2}$ peak. XPS spectra of Be $1s$ recorded with a photon energy of 460 eV and W $4f$ recorded with 380 eV after experimental steps are shown in figures 2(a) and 2(b).

After deposition of W on Be, three peaks can already be identified by eye in the W $4f$ spectrum. On both sides of the main peak shoulders are visible (Fig. 2(a), spectrum W on Be). The shoulder on the low BE side is located at 30.9 eV. This peak is assigned to the Be-W alloy at the interface of W and Be. The second shoulder at 32.0 eV is assigned to a ternary compound consisting of Be, O and W. A third function is set to the binding energy of metallic W at 31.4 eV. Using these three functions with a fixed binding energy for metallic W the spectral shape cannot be reproduced, requiring to include a fourth function in the fit procedure. The fourth peak is located 31.3 eV. Using these four functions provides an excellent fit of the recorded spectrum, as shown in Fig. 3. The function located at 31.3 eV is assigned to the surface core level (SCL) of metallic W. Therefore the surface core level shift (SCLS) is determined to be -0.1 eV. Unfortunately no literature data is available for the SCLS of polycrystalline W. Nevertheless, the assignment of this peak is viable, since W shows a surface shift to lower binding energies, according to calculations by e.g. Aldén et al. [12] and experiments on W single crystals,

e.g. by Wertheim et al. [13]. The high surface/bulk intensity ratio for the metallic W, as determined from the peak fit, is interpretated such that metallic W is predominantly present at the very surface, whereas W bound to Be or O is located below the first layer.

After the subsequent alloying step, in both Be 1s and W 4f spectral regions Be_2W is clearly visible (s. Fig. 2(a) & 2(b), spectra 'Be_2W'). In the W 4f region the peak is well represented by a single fit function positioned at 30.9 eV and is assigned to Be_2W. In the corresponding Be 1s spectrum the large peak can be split into two contributions: The main contribution is here also the alloy at 111.1 eV and a smaller contribution originates from metallic Be at 111.8 eV. One additional broad peak is visible with its maximum at 114.1 eV. Since there are no ternary phases with W visible in the W 4f spectrum, the only possible assignment is BeO. This is supported by O visible in the survey scans. The O signal originates from O adsorbed during alloy formation and sample transfer and measurement from the residual gas. This cannot be avoided due to the high oxophily of Be, even under the present vacuum conditions.

Implantation of O at 1 kV acceleration voltage induces a significant change in both the W 4f and Be 1s spectra. Peak fitting analysis of the W spectrum reveals six doublets: W and its SCL at 31.4 eV and 31.3 eV, Be_2W at 30.9 eV, WO_3 at 35.9 eV and two doublets which are assigned to ternary phases at 31.9 eV and 36.6 eV (for assignment, see section 4).

The annealing step at 600 K for 30 min leads to a reduction of W, visible in the loss of intensity at binding energies above 34 eV (Fig. 2(a), spectrum '600 K'). Only one doublet is still visible. Peak fitting reveals only one contribution assigned to the alloy at 31.1 eV. In the Be 1s spectrum a small signal at the position of Be_2W is present (Fig. 2(b), spectrum '600 K'). The second peak at 114.8 eV in the Be 1s is assigned to BeO, since no ternary compounds are observed in the W spectrum.

After the first implantation of O with 500 V major changes are observable in both W 4f and Be 1s spectral regions. Compared to the O implantation with 1 kV, two additional peak pairs can be identified. The first is located at 34.6 eV and is assigned to the substoichiometric tungsten oxide WO_{3-x}, the second at 33.0 eV, assigned to tungsten dioxide WO_2. Most intensity is distributed over the energy region above 34 eV. In this region, only W in the oxidation state VI can be found. In the Be 1s spectrum only one broad, asymmetric peak is observed. Fitting based on the information from the W 4f

region reveals three components: Two components from ternary compounds and BeO. Thus, the ternary compounds can be found in both, the Be 1s and the W 4f spectra.

The second O implantation with 500 V leads to the formation of the same compounds. In the W 4f spectrum the main intensity of the two peaks visible at binding energies above 34.0 eV originates here from WO_3 (Fig. 2(a), spectrum 'O^+ 500 eV II'). Only a small contribution of $BeWO_4$ can be observed. In the Be 1s spectrum, again only one broad peak is present which is shifted to lower binding energies compared to the first 500 V implantation (Fig. 2(b), spectrum 'O^+ 500 eV I'). This shift is attributed to a significantly lower amount of $BeWO_4$, which is in good agreement with the observations in the W 4f region.

4 Discussion

In the literature two ternary compound types are found which contain W, O and a third element: The tungsten bronzes with the stoichiometry M_xWO_3 with x ranging from 0–1, and the tungstates M_2WO_4. No literature data is available for these ternary compounds with M = Be. For tungstates literature data for various compounds is available. The chemically most similar element to Be is Al. Therefore, literature values for $Al_2(WO_4)_3$ are considered for comparison with the binding energies of $BeWO_4$ in this work. For $Al_2(WO_4)_3$ binding energies for W in WO_4^{2-} are available. Biloen and Pott report a binding energy of 36.5 eV [14] for the tungstate, Ng and Hercules 35.4 eV [15], Salvati et al. 36.1 eV [16], Barrault et al. 36.2 eV for Al_2O_3/WO_3 [17] and Grünert et al. 36.7 eV [18]. Although the variation between these values is quite high, all authors report binding energies similar or higher compared to their respectively cited WO_3 binding energies. Based on these references, the ternary compound found at 36.6 eV is assigned to beryllium tungstate $BeWO_4$, with the anion WO_4^{2-} as building block.

Assignment of the second binding energy of 31.9 eV found by peak fitting is more difficult, since literature on XPS investigations of tungsten bronzes is scarce. For sodium W bronzes data can be found: Biloen and Pott report in their work investigations on two different sodium tungsten bronzes [14]. We compare our findings with the results of their work, since here binding energies can be found for $Na_{0.1}WO_3$ and $Na_{0.6}WO_3$, although we are aware of the differences of these to elements. Be and Na have a difference of 0.64 in electronegativity on the Pauling scale. Biloen and Pott found a binding energy

of 35.8 eV for $Na_{0.1}WO_3$ and 36.0 eV for $Na_{0.6}WO_3$, which is 0.2 eV lower or the same as their reported binding energy for WO_3 [14]. Our binding energy of 31.9 eV is 4.0 eV lower than the binding energy of WO_3. Following the trend, assignment of the binding energy of 31.9 eV to $BeWO_3$ is viable. Nonetheless, further investigations have to be conducted to justify this assignment.

In experiments conducted in thermal equilibrium with Be on WO_3, we found $BeWO_4$ at the same binding energy as in the implantation experiments described above. In thermal experiments $BeWO_4$ is observed only for temperatures above 600 K. Contrary, we observe here that $BeWO_4$ is formed by ion bombardment already at r.t. This finding can be explained by two effects: First O is implanted directly in to the Be_2W lattice, leading to forced insertion of O into the crystal lattice of Be_2W. The second effect to be considered here is ion beam mixing. The implanted ions dissipate their energy to atoms in the lattice, allowing them to overcome the diffusion barrier and move to more favorable positions in the crystal lattice. The so-formed crystal structure is not comparable with the crystal structure formed by reactions in thermal equilibrium. In thermal experiments, beginning decomposition of $BeWO_4$ is observed at a temperature of 1073 K and above, while the phase formed by ion implantation decomposes already completely at 600 K. This difference in decomposition temperature again points to different crystal structures. After decomposition, O stays bound in the sample as BeO, which is deducted from the loss of intensity contributions from oxidic species in the W $4f$ spectra and the remaining oxidic contribution in the Be $1s$ spectra.

Oxidic compounds are formed within implantation range. No indication for diffusion into the bulk is found, since in the spectra of the Be $1s$ region, Be_2W is still visible in the spectra recorded with photon energies of 610 and 820 eV, as shown in Fig. 4. This Fig. shows the spectra of the Be $1s$region after the 1^{st} O-implantation with 500 V recorded at different photon energies. In the spectra recorded at 235, 350 and 460 eV no Be_2W is visible. In the spectrum recorded at 610 eV a very small contribution of Be_2W can be identified. This contribution is more pronounced in the spectrum recorded at 820 eV. The progression of this contributions clearly shows, that in the surface near region all Be can be found in oxidic states, while in the deeper regions Be still occurs as Be_2W. This is explained by the lack of oxygen for complete oxidation of Be at greater depth.

5 Summary

Oxygen implantation with an acceleration voltage of 500 V is sufficient to form ternary compounds Be_xWO_3 and $BeWO_4$ at r.t. due to ion beam mixing and energy deposition. Formation of compounds is only visible in depths were oxygen is available. No indication of oxygen diffusion is found at r.t. Annealing at 600 K decomposes the ternary compounds. After the decomposition oxygen remains bound in the sample as BeO. Repetitive implantations of oxygen lead again to the formation of ternary compounds.

Acknowledgements

The help of Thanh-Vinh Phan and Heike Löchel during beam time is highly appreciated. This work has partially been funded in the frame of the FEMaS project within the European Atomic Energy Community's Seventh Framework Programme (FP7 / 2007-2011) under Grant Agreement 224752.

References

[1] G. Federici, A. Loarte, G. Strohmayer, *Plasma Phys. Contol. Fusion.* **2003**, *45*(9), 1523–1547

[2] Ch. Linsmeier, K. Ertl, J. Roth, A. Wiltner, K. Schmid, F. Kost, S.R. Bhattacharyya, M. Baldwin, R.P. Doerner, *J. Nucl. Mater.* **2007**, *363-365*, 1129 – 1137

[3] M. Köppen, Ch. Linsmeier, *to be published* **2011**

[4] F. Kost, Ch. Linsmeier, M. Oberkofler, M. Reinelt, M. Balden, A. Herrmann, S. Lindig, *J. Nucl. Mater.* **2009**, *390-391*, 975 – 978

[5] NIST Mass Spec Data Center, S.E. Stein (director), *NIST Chemistry Webbook, NIST Standard Reference Database Number 69*, Chapter Mass Spectra, National Institute of Standards and Technology, Gaithersburg MD **2011**

[6] W. Eckstein, R. Dohmen, A. Mutzke, R. Schneider, *SDTrimSP: A Monte-Carlo Code for Calculating Collision Phenomena in Randomized Targets*, Max-Planck-Institut für Plasmaphysik, IPP-Report 12/3 **2007**

[7] W. Eckstein, *Computer Simulation of Ion-Solid Interactions*, Springer Series in Materials Science, Vol. 10, Springer, Berlin **1991**

[8] M.P. Seah, W.A. Dench, *Surf. Interface Anal.* **1979**, *1*, 2–11

[9] J. J. Yeh, I. Lindau, *At. Data Nucl. Data Tables* **1985**, *32*(1), 1 – 155

[10] S. Tougaard, P. Sigmund, *Phys. Rev. B* **1982**, *25*(7), 4452–4466

[11] S. Doniach, M. Šunjić, *J. Phys. C: Solid State* **1970**, *3*(2), 285–291

[12] M. Aldén, H. L. Skriver, B. Johansson, *Phys. Rev. B* **1994**, *50*(16), 12118–12130

[13] G. K. Wertheim, P. H. Citrin, J. F. van der Veen, *Phys. Rev. B* **1984**, *30*(8), 4343–

[14] P. Biloen, G. T. Pott, *J. Catal.* **1973**, *30*(2), 169–174

[15] T. K. Ng, D. M. Hercules, *J. Phys. Chem.* **1976**, *80*(19), 2094–2102

[16] L. Salvati, L. E. Makovsky, J. M. Stencel, F. R. Brown, D. M. Hercules, *J. Phys. Chem.* **1981**, *85*(24), 3700–3707

[17] J. Barrault, M. Boulinguiez, C. Forquy, R. Maurel, *Appl. Catal.* **1987**, *33*(2), 309 – 330

[18] W. Grünert, E. S. Shpiro, R. Feldhaus, K. Anders, G. V. Antoshin, Kh. M. Minachev, *J. Catal.* **1987**, *107*(2), 522 – 534

Graphs and tables

Table 1: Experimental photon energies, respective photoelectron kinetic energies and the related inelastic mean free paths (IMFP) according to Seah and Dench [8]

photon energy $h\nu$ [eV]			approximate kinetic energy	IMFP
W $4f$	Be $1s$	O $1s$	of photoelectrons [eV]	[nm]
73	155	570	45	0.4
155	235	655	125	0.6
260	350	740	225	0.8
380	460	870	325	1.0
530	610	1040	475	1.2
740	820	1235	685	1.4

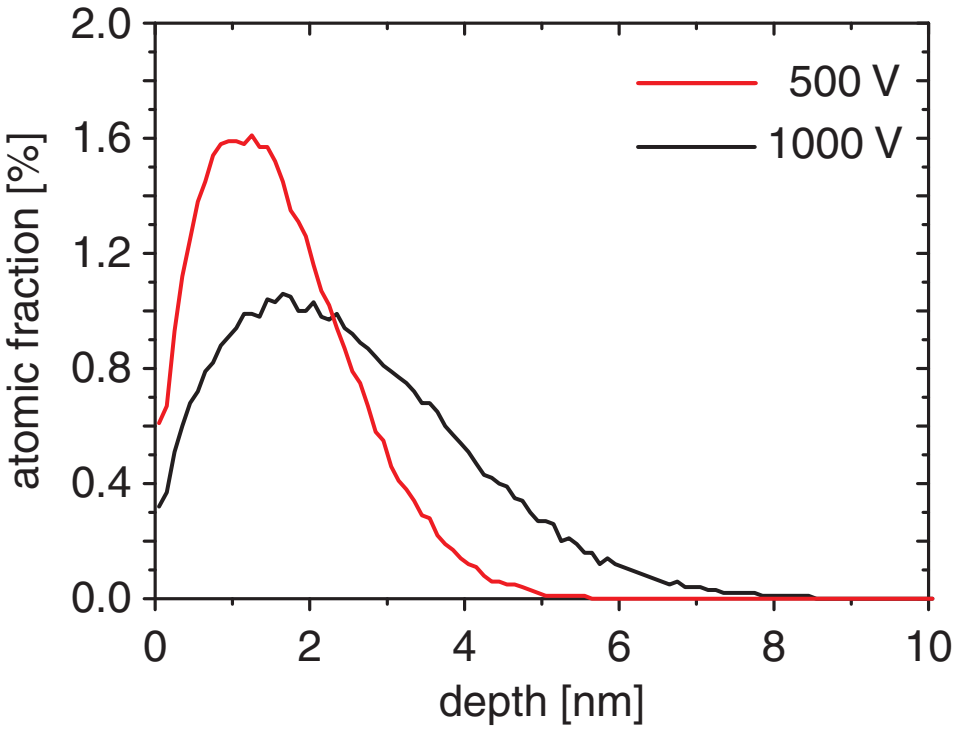

Figure 1: Simulated depth distribution of implanted oxygen in Be_2W, calculated with SDTrim.SP [6, 7] for implantation energies of 500 and 1000 eV and fluences of $5 \cdot 10^{14}$ cm^{-2}.

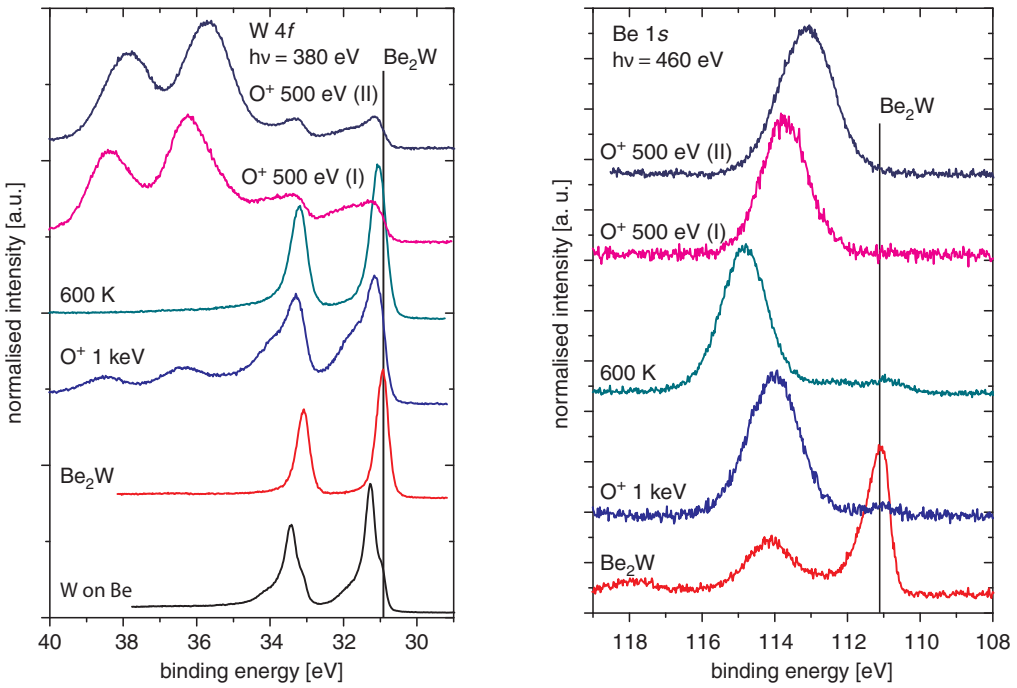

(a) W $4f$ spectra recorded with $h\nu$ = 380 eV

(b) Be $1s$ spectra recorded with $h\nu$ = 460 eV

Figure 2: Spectra of the W $4f$ and Be $1s$ core levels recorded after the indicated experimental step.

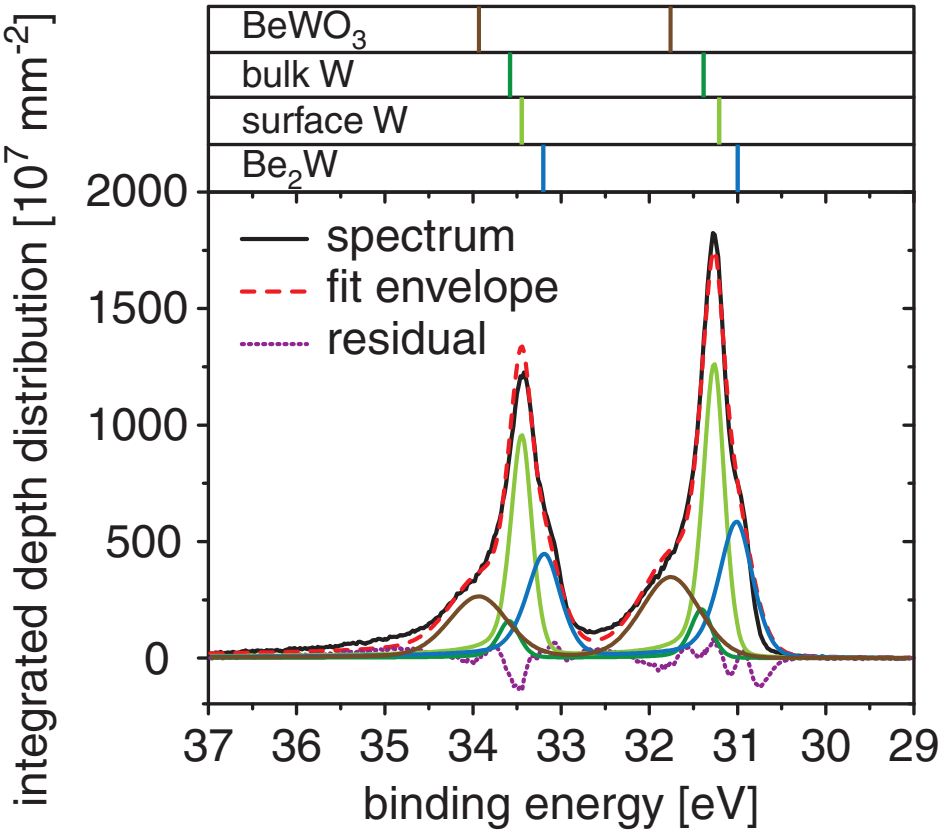

Figure 3: Fit of the W 4f region after evaporation of W on Be, recorded with a photon energy of 380 eV. Peak assignment is shown in the upper section of the graph.

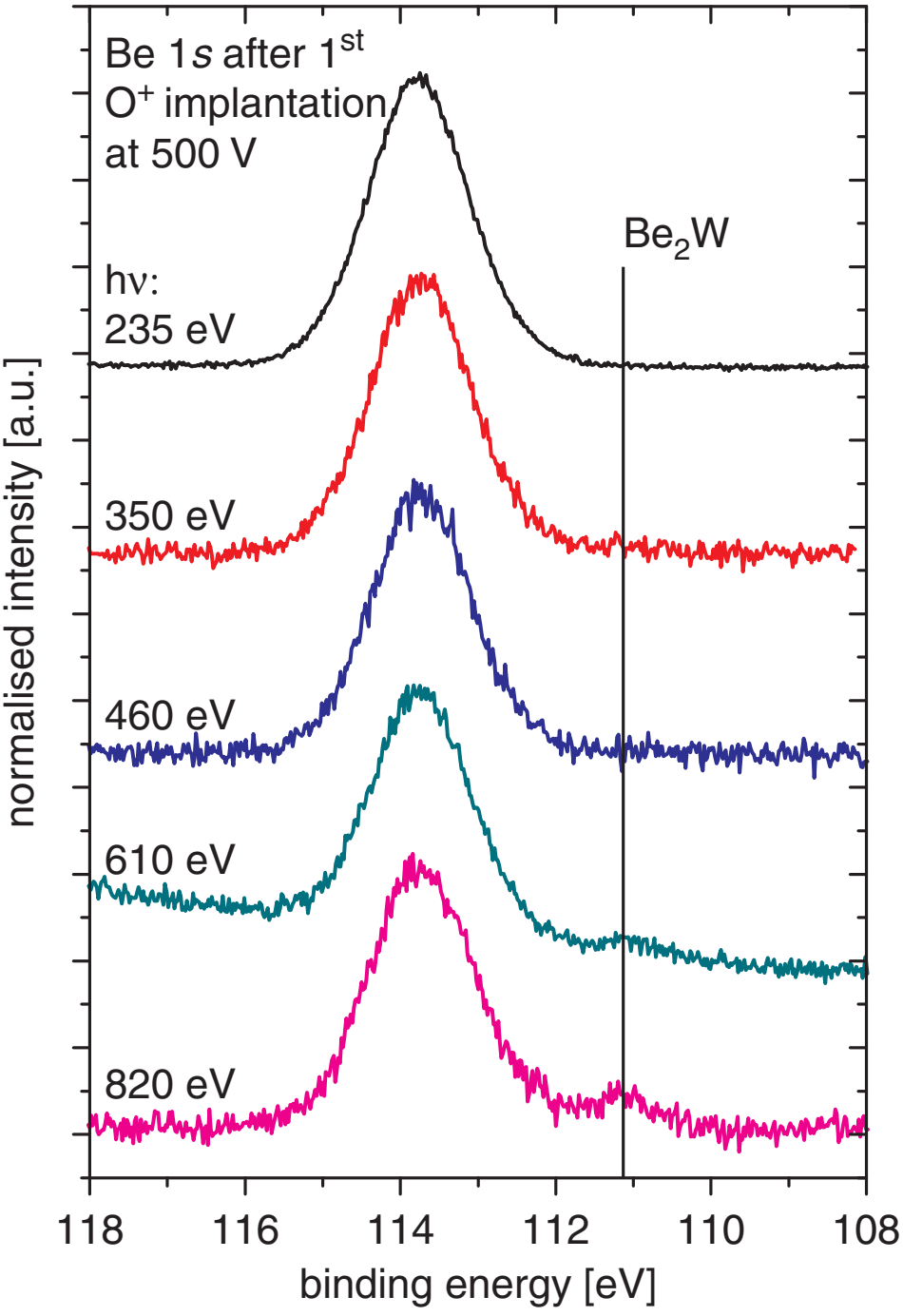

Figure 4: Be 1s spectra recorded after the first implantation of oxygen ions with an acceleration voltage of 500 V. The higher the photon energy, hν, the more photoelectrons from greater depths contribute to the detected intensity.